The Journal of Neuroscience, November 1, 1998, *18*(21):8590–8604

Defining Affinity with the $GABA_A$ Receptor

Mathew V. Jones,[1] **Yoshinori Sahara,**[1,2] **Jeffrey A. Dzubay,**[1] **and Gary L. Westbrook**[1,3]

[1]*Vollum Institute and* [3]*Department of Neurology, Oregon Health Sciences University, Portland, Oregon 97201, and* [2]*Department of Physiology, Faculty of Dentistry, Tokyo Medical and Dental University, Tokyo 113, Japan*

At nicotinic and glutamatergic synapses, the duration of the postsynaptic response depends on the affinity of the receptor for transmitter (Colquhoun et al., 1977; Pan et al., 1993). Affinity is often thought to be determined by the ligand unbinding rate, whereas the binding rate is assumed to be diffusion-limited. In this view, the receptor selects for those ligands that form a stable complex on binding, but binding is uniformly fast and does not itself affect selectivity. We tested these assumptions for the $GABA_A$ receptor by dissecting the contributions of microscopic binding and unbinding kinetics for agonists of equal efficacy but of widely differing affinities. Agonist pulses applied to outside-out patches of cultured rat hippocampal neurons revealed that agonist unbinding rates could not account for affinity if diffusion-limited binding was assumed. However, direct measurement of the instantaneous competition between agonists and a competitive antagonist revealed that binding rates were orders of magnitude slower than expected for free diffusion, being more steeply correlated with affinity than were the unbinding rates. The deviation from diffusion-limited binding indicates that a ligand-specific energy barrier between the unbound and bound states determines $GABA_A$ receptor selectivity. This barrier and our kinetic observations can be quantitatively modeled by requiring the participation of movable elements within a flexible GABA binding site.

Key words: ligand-gated channels; kinetics; selectivity; molecular modeling; synapse; thermodynamic

Interactions between neurotransmitters and receptors are often assessed by analyzing the equilibrium concentration–response relationship (Segel, 1976; Pallotta, 1991). However, the applicability of equilibrium conditions is problematic for fast chemical synapses in which the concentration of neurotransmitter rises and falls rapidly (Magleby and Stevens, 1972; Katz and Miledi, 1973; Lester et al., 1990; Clements et al., 1992). Transmitter binding primarily occurs early in the synaptic response when the free transmitter concentration is high, whereas unbinding primarily occurs as transmitter is decaying or after it has been cleared. Furthermore, the EC_{50} does not reflect any individual transition but is instead an indicator of the total time spent in all channel states (for review, see Jones and Westbrook, 1996). The binding steps probably determine the fraction of receptors activated and the likelihood of intersynaptic communication (Barbour and Häusser, 1997), whereas the gating and unbinding steps determine the response duration. A quantitative understanding of the contributions of binding, gating, and unbinding in shaping synaptic transmission is greatly facilitated by a nonequilibrium approach.

Binding and unbinding kinetics also provide functional (and possibly structural) information about the binding site, which is especially important given the scarcity of crystallographic information for ligand-gated channels. For example, the binding of ACh to nicotinic ACh receptors is almost as fast as that predicted if the rate-limiting step is the diffusion of ligand into the binding site (Colquhoun and Sakmann, 1985; Colquhoun and Ogden, 1988; Papke et al., 1988; Jackson, 1989; Auerbach, 1993; Franke et al., 1993; Sine et al., 1995; Akk and Auerbach, 1996). Such efficient binding suggests that there are few significant barriers to binding and that there is an almost perfect "fit" between agonist and the activated receptor (Jackson, 1989). Binding at AMPA, NMDA, and $GABA_A$ receptors appears to be somewhat slower than that for nicotinic ACh (nACh) receptors (Clements and Westbrook, 1991; Jonas et al., 1993; Celentano and Wong, 1994; Jones and Westbrook, 1995; Raman and Trussell, 1995; Häusser and Roth, 1997), although the structural and functional significance of slower binding at these receptors remains unknown.

One approach to understanding the nature of affinity and selectivity is to compare binding and unbinding between different ligands at the same receptor. For nACh and NMDA receptors, affinity was found to be inversely related to the unbinding rate (Colquhoun et al., 1977; Colquhoun and Sakmann, 1985; Papke et al., 1988; Benveniste et al., 1990a,b; Benveniste and Mayer, 1991; Lester and Jahr, 1992; Pan et al., 1993; Akk and Auerbach, 1996). However, there is also evidence that differences in affinity between agonists at nACh and $GABA_A$ receptors are more strongly determined by the binding rate (Sine and Steinbach, 1986; Jones and Westbrook, 1995; Zhang et al., 1995; Akk and Auerbach, 1996). Here, we investigated the binding and unbinding of $GABA_A$ receptor ligands with affinities spanning several orders of magnitude, using fast solution exchange methods in outside-out patches. Unbinding rates could not account for affinity if diffusion-limited binding was assumed. In contrast, affinity could be predicted from the binding rates that were much slower than the diffusion limit. These data indicate that an energy-requiring event, such as a conformational change of the GABA binding site, precedes or accompanies binding.

Received June 19, 1998; revised Aug. 3, 1998; accepted Aug. 11, 1998.

M.V.J. was sponsored in part by the American Epilepsy Society with support from the Milken Family Medical Foundation. Y.S. was supported by a grant from the Japanese Ministry of Education, Science, and Culture. This work was supported by National Institutes of Health Grants F32 NS09716 (M.V.J.) and NS26494 (G.L.W.). We thank Drs. Jeff Diamond, Craig Jahr, and Tom Otis for helpful discussions and Jeff Volk for culture of hippocampal neurons. Special thanks to Dr. Gary Yellen for an invaluable conversation.

Correspondence should be addressed to Dr. Mathew V. Jones, The Vollum Institute, Oregon Health Sciences University, L474, 3181 Southwest Sam Jackson Park Road, Portland, OR 97201.

MATERIALS AND METHODS

Cell culture and recording. Cell culture methods were identical to those described previously (Jones and Westbrook, 1995). Outside-out patches were excised from neonatal rat hippocampal neurons maintained in culture from 1 to 4 weeks. Recordings were made under voltage-clamp ($V_{hold} = -60$ mV; 25°C). Internal pipette solutions contained (in mM): 144 KCl, 1 $CaCl_2$, 3.45 BAPTA, 10 HEPES, and 5 Mg_2ATP, at pH 7.2 and 315 mOsm. The standard external solution contained (in mM): 140 NaCl, 2.8 KCl, 1 $MgCl_2$, 1.5 $CaCl_2$, 10 HEPES, 10 D-glucose, 0.01 CNQX, and 0.001 strychnine, at pH 7.4 and 325 mOsm. When β-alanine (100 mM) or 4,5,6,7-tetrahydroisoxazolo[5,4-c]pyridin-3-ol HCl (THIP; 50 mM) were used, the NaCl concentration was adjusted to 110 or 60 mM (plus sucrose) to maintain a constant osmolarity. $GABA_A$ receptor agonists and antagonists were added to the external solution and applied to whole cells or patches using multibarreled flow pipes (Vitro Dynamics, Rockaway, NJ) mounted on a piezoelectrical bimorph (Vernitron, Bedford, OH). Two computer-controlled voltage sources in series with the bimorph were used to control solution exchanges. Whole-cell solution exchange required ~100 msec, whereas the 10–90% rise and fall times of liquid junction currents at the open pipette tip after each patch experiment were <1 msec. Currents were filtered at 1–5 kHz using a four-pole Bessel filter and were acquired at greater than or equal to twice the filter frequency (AxoBASIC; Axon Instruments, Foster City, CA). Muscimol, THIP, and 2-(3-carboxypropyl)-3-amino-6-(4-methoxyphenyl)pyridazinium bromide (SR-95531) were obtained from Research Biochemicals (Natick, MA). GABA, β-alanine, and all other chemicals were from Sigma (St. Louis, MO).

Estimation of unbinding rates. We used a modification of a previously established Markov model of $GABA_A$ receptor kinetics (Jones and Westbrook, 1995, 1997) to estimate agonist unbinding rates. Responses from several experiments were averaged together before performing least-squares fitting of the data. Fitting and calculation of confidence limits were performed using SCoP (Simulation Resources, Berrien Springs, MI). The addition of transitions between desensitized states that entail a net counterclockwise movement at steady state allows more accurate fitting of slow components (Jones and Westbrook, 1995) and does not qualitatively alter our conclusions. Data are reported as mean ± SEM unless otherwise noted. Kinetic differences were determined by two-tailed *t* tests or by one-way ANOVA followed by *post hoc* tests when several groups were compared.

A general model of binding and unbinding kinetics. Because rate constants derived from predefined Markov models may depend strongly on the structure of the model chosen, we also used a more general format for describing ligand–receptor interactions. This approach is based on the assumptions common to mass action treatments of binding and enzyme kinetics and requires no a priori knowledge of rate constants or the number and cooperativity of ligand binding sites. We assume that channels are independent and that each channel contains N binding sites. By analogy with Hodgkin–Huxley formalism (Hille, 1992), binding to each site (n) can be described by the reaction:

$$\text{Unbound}_n \underset{\upsilon_n}{\overset{\omega_n}{\rightleftharpoons}} \text{Bound}_n \quad \text{or} \quad 1 - P_n \underset{\upsilon_n}{\overset{\omega_n}{\rightleftharpoons}} P_n, \tag{1}$$

so that $\omega_n = [A]k_{on_n}$ and $\upsilon_n = k_{off_n}$, where P_n is the probability of being bound (occupancy), $[A]$ is the ligand concentration, and k_{on} and k_{off} are the rate constants for binding and unbinding. When the ligand concentration is changed, the occupancy will relax over time to a new value according to:

$$P_n(t) = P_{n\infty} - (P_{n\infty} - P_{n0})e^{-t/\tau_n}, \tag{2}$$

where the occupancy is P_{n0} initially (at $t = 0$) and $P_{n\infty}$ at steady state (as $t \rightarrow \infty$):

$$P_{n\infty} = \frac{\omega_n}{\omega_n + \upsilon_n}. \tag{3}$$

The microscopic affinity constant K_n can be defined by solving Equation 3 for the concentration at half-occupancy, yielding:

$$K_n = k_{off_n}/k_{on_n}. \tag{4}$$

The probability of receptor saturation (P_{sat}) is the product of the individual occupancies:

$$P_{sat} = \prod_{n=1}^{N} P_n = P_1P_2 \ldots P_N, \tag{5}$$

and if all sites are equal and independent (i.e., $\omega_1 = \omega_2 \ldots \omega_n$ and $\upsilon_1 = \upsilon_2 \ldots \upsilon_n$), then:

$$P_{sat} = P_n^N. \tag{6}$$

As with Equation 4, solving Equation 6 for the concentration of half-saturation defines the macroscopic affinity constant K_N, which is a function of both the microscopic affinity and the number of sites N:

$$K_N = \frac{K_n}{(2^{1/N} - 1)}. \tag{7}$$

Finally, the equilibration time constant τ_n at each site is given by:

$$\tau_n = \frac{1}{\omega_n + \upsilon_n} \quad \text{or} \quad \frac{1}{\tau_n} = [A]k_{on_n} + k_{off_n}, \tag{8}$$

whereas the macroscopic equilibration will have N components. The version of Equation 8 on the right is particularly useful because $1/\tau_n$ is a linear function of concentration, the slope and intercept of which are the microscopic rate constants.

Additional allowances are required to model agonist-activated currents. For example, agonist efficacy could be described using proportionality constants relating occupancy to open probability, and desensitization could be described by Hodgkin–Huxley-style inactivation parameters. Here, however, we will use the relations as given above and focus our attention on the binding and unbinding of the competitive antagonist SR-95531 that is not expected to cause channel gating or desensitization (Hamann et al., 1988; Jones and Westbrook, 1997; but see Ueno et al., 1997). We first consider a mechanism in which antagonist binding to any one of the binding sites is sufficient to prevent channel opening. For equal and independent sites, the probability that a channel will be available for activation (i.e., all sites remain free of antagonist) is thus:

$$P_{avail} = (1 - P_n)^N. \tag{9}$$

For unequal sites, Equation 9 would be expanded to include the individual parameters (compare Eq. 5). This treatment can easily be extended to the case in which all sites must be occupied by antagonist to block the channel, but such a model did not accurately describe our data.

Measuring agonist binding rates. When an agonist and competitive antagonist are rapidly and simultaneously applied to a patch, the resulting peak current is smaller than that produced by agonist alone because some channels initially bind antagonist and become blocked. We refer to such instantaneous competition as a "race" experiment (e.g., Clements et al., 1992; Diamond and Jahr, 1997). For a single site per receptor at which the two ligands compete (see Results):

$$\frac{R_{ag}}{R_{ant}} = \frac{\omega_{ag}}{\omega_{ant}} \quad \text{or} \quad R_{ag} = R_{ant}\frac{\omega_{ag}}{\omega_{ant}}, \tag{10}$$

and:

$$I_{race} = \frac{R_{ag}}{R_{ag} + R_{ant}}, \tag{11}$$

where R is the fraction of receptors bound with either agonist or antagonist, ω is the binding rate (i.e., the concentration times a rate constant), and I_{race} is the ratio of peak current produced during the race to that produced by agonist alone. Dividing both the numerator and denominator of Equation 11 by R_{ag}, substituting from Equation 10, and rearranging yield:

$$k_{on(ag)} = \frac{[ant]k_{on(ant)}}{[ag]\left(\frac{1}{I_{race}} - 1\right)}, \tag{12}$$

where $k_{on(ag)}$ and $k_{on(ant)}$ are the binding rate constants and [ag] and [ant] are the concentrations of agonist and antagonist. Therefore, if the antagonist binding rate is known and unbinding is slow relative to the

current rise time, then Equation 12 can be used to measure the agonist binding rate by performing a race experiment.

Diffusion and energetics. If every encounter between diffusing ligand molecules and the binding site results in ligand attachment, the binding reaction is said to be diffusion-limited. We estimated the theoretical rate constant for such a process by assuming (1) that the radius of the encounter (r) is approximately the same as the size of a GABA molecule (~4 Å), (2) that the binding site can be approached from any direction, and (3) that the ligand diffusion coefficient (D) is 3×10^{-6} cm^2 sec^{-1} (Busch and Sakmann, 1990). The rate constant (k_{diff}) for a diffusion-limited binding reaction would then be (Freifelder, 1982; Hille, 1992):

$$k_{diff} = 4\pi r D N_A = 9.1 \times 10^9 \ M^{-1} \ sec^{-1}, \quad (13)$$

where N_A is Avogadro's number. Other equally plausible assumptions could give values for k_{diff} greater or smaller than that of Equation 13. However, we will show in the Results that such variation is negligible in comparison with the measured differences in agonist binding rates.

When ligand binding is not diffusion-limited, only encounters possessing sufficient energy result in productive binding. The Arrhenius equation (Freifelder, 1982) relates this activation energy (E_a) to the ratio of observed and diffusion-limited binding rates:

$$E_a = -RT \ln\left(\frac{k_{on}}{k_{diff}}\right), \quad (14)$$

where R is the gas constant and T is the absolute temperature.

Physical modeling of the agonist binding reaction. We used rudimentary molecular modeling to simulate the experimentally determined energetics of the binding/unbinding reaction. Both the agonists and the binding site were assumed to consist of "particles" that undergo purely van der Waals-like interactions with each other. Each agonist was modeled as two particles representing the agonist endpoints, separated by a fixed length [estimated from minimum energy conformations *in vacuo* using ChemOffice (CambridgeSoft, Cambridge, MA)]. The binding site was modeled either as being rigid (i.e., two particles a fixed distance apart) or as being flexible (two rigid anchor particles separated by a distance L_{site}, associated with two movable arm particles). For the rigid model, unbound agonists were assumed to be associated with additional movable particles representing waters of hydration. The changing energy of the system as ligand binding progressed stepwise was calculated using the Lennard–Jones potential equation (Freifelder, 1982; Morris et al., 1996):

$$\text{Energy} = \frac{C_{12}}{r^{12}} - \frac{C_6}{r^6}, \quad (15)$$

where r is the distance between any two particle centers (in angstroms). The empirical coefficients C_{12} and C_6 are related to the repulsive and attractive intermolecular forces, respectively, and are defined in terms of the equilibrium distance between particle centers (r_{eqm}) and the depth of the energy well (ϵ) occurring at that distance (Morris et al., 1996):

$$C_6 = 2\epsilon r_{eqm}^6 \quad \text{and} \quad C_{12} = \epsilon r_{eqm}^{12}. \quad (16)$$

The total energy of the system at each step was the sum of all pairwise particle interaction energies. For simplicity, all particles and movements were coplanar for a rigid site and collinear for a flexible site. Model parameters were optimized for all agonists simultaneously using a simplex algorithm (Nelder and Mead, 1965) to minimize the sum of squared errors in energy. Simulation programs were written in MATLAB (The Math Works, Natick, MA) and run on Macintosh computers.

RESULTS

Deactivation depends on agonist affinity whereas gating does not

The decay of the IPSC represents the relaxation of $GABA_A$ receptors from ligand-bound to unbound states. Although oscillations between open and desensitized states are important in shaping this deactivation, the rate of ligand unbinding must also contribute (Jones and Westbrook, 1995, 1996, 1997). To assess this contribution, we examined currents activated by saturating pulses of a series of $GABA_A$ receptor agonists (GABA, muscimol, THIP, and β-alanine) to outside-out patches from rat hippocampal neurons. Figure 1*A* shows that the duration of deactivation after brief (5 msec) agonist pulses depends strongly on the agonist. The time constants (τ_{fast} and τ_{slow}) and the relative contribution of the fast decay component ($\%_{fast}$) were 15 ± 2 and 372 ± 39 msec (50 ± 6%), respectively, for muscimol (n = 4); 14 ± 2 and 233 ± 17 msec (64 ± 3%) for GABA (n = 18); and 12 ± 2 and 109 ± 32 msec (87 ± 4%) for THIP (n = 4). In four of six patches, β-alanine currents were best fit by a single exponential of 9 ± 2 msec. In contrast to the agonist-dependent

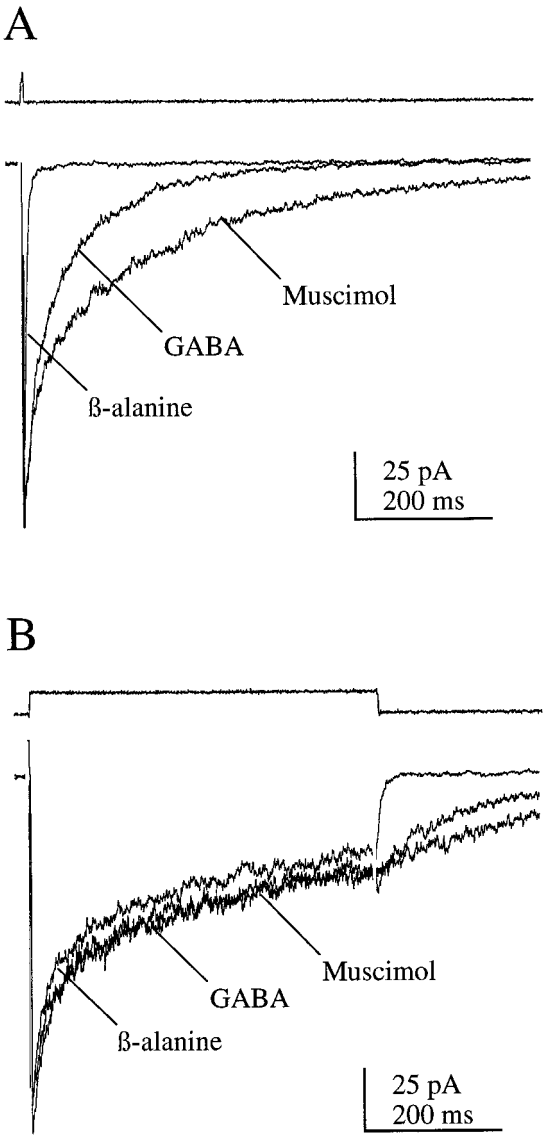

Figure 1. Unbinding from the $GABA_A$ receptor is agonist-specific, but gating is not. *A*, When brief (5 msec) and saturating agonist pulses were applied to outside-out patches, the time course of current decay (deactivation) depended on the agonist used. Pulses of GABA (10 mM) and either muscimol (10 mM) or β-alanine (100 mM) were alternated on a single patch. The *lower traces* are the averages of more than five records. The *top traces* are the liquid junction currents recorded at the open pipette tip at the end of the experiment and illustrate the speed of solution exchange. Piezoelectrical artifacts have been blanked. *B*, The amplitudes and time courses (desensitization) of currents during long (505 msec) pulses of GABA, muscimol, or β-alanine were indistinguishable from each other, suggesting that channel gating is similar across different agonists. However, the deactivation time course after agonist removal was agonist-specific, suggesting that the rate of return to the unbound state depends on agonist structure.

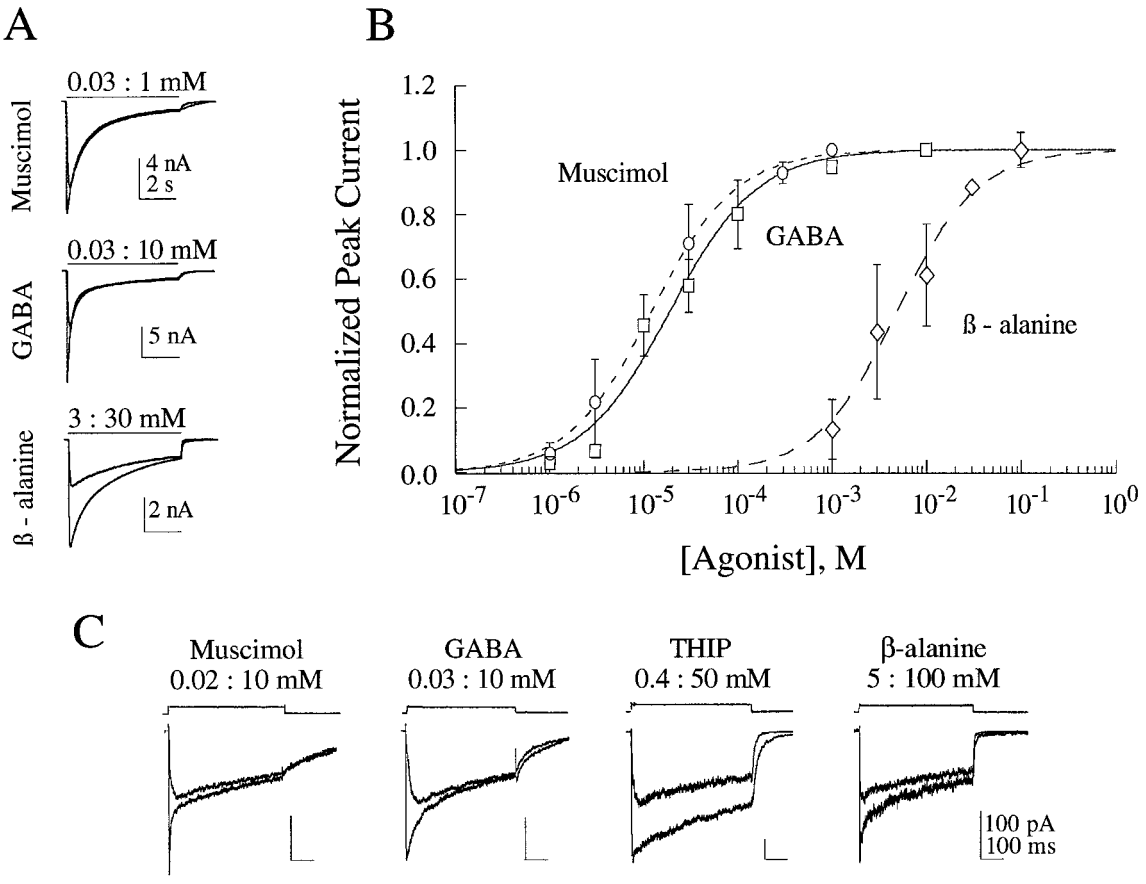

Figure 2. Agonists span a wide range of affinities. *A*, Whole-cell currents were evoked by submaximal and maximal applications of agonists, at the concentrations shown *above* the *traces*. The *horizontal lines* show the duration of agonist application. *B*, Concentration-response data from experiments like those shown in *A* were fit to the normalized form of the Hill equation: $I/I_{max} = 1/(K_H/[A]^N + 1)$ (Segel, 1976). I/I_{max} is the fraction of the maximal current, N is the number of agonist binding sites per receptor, and K_H is a constant reflecting both the concentration at the half-maximal response and the degree of cooperativity between sites. Note that K_H must be expressed as a concentration raised to the power of N for units to balance. The fitted parameters are given in the text. *C*, A more precise estimate of EC_{50} was obtained by alternating approximately half-maximal (giving between 45 and 55% of the maximal peak current) and maximal concentrations at outside-out patches. The differences in desensitization kinetics reflect patch-to-patch variability and were not statistically significant (see Fig. 1*B*). The *upper traces* are the liquid junction currents.

deactivation, current amplitudes and kinetics were indistinguishable during long (505 msec) pulses that maintained the receptor in the fully bound state (Fig. 1*B*). Desensitization was fitted with two exponential components for all agonists [e.g., for GABA, 20 ± 4 msec, 786 ± 40 msec, and 40 ± 3% (n = 18)]. Deactivation at the end of long agonist pulses was agonist-dependent and followed the same rank order as that for brief pulses (Fig. 1*B*). Because the agonists produced indistinguishable currents under saturating conditions (i.e., they appear to have identical efficacy), any kinetic differences were presumably caused by binding or unbinding. Thus, agonist-dependent deactivation results from agonist-specific unbinding.

The role of unbinding kinetics in deactivation and receptor affinity

Affinity describes the probability of finding a ligand molecule bound to the receptor for a given ligand concentration, whereas selectivity refers to differences in affinity between ligands. Both measures depend on the time that each ligand spends in the binding site but also on the likelihood that the ligand becomes bound in the first place. To understand the factors governing the entry and exit of ligands at the binding site, we began by measuring the apparent affinities of muscimol, GABA, and β-alanine from peak whole-cell concentration–response plots using the Hill equation (Fig. 2*A*,*B*). For muscimol, K_H was 10.9 μM^N, and N was 0.96; for GABA, K_H was 15.4 μM^N, and N was 0.93; and for β-alanine, K_H was 5.9 mM^N, and N was 1.0. Caution is necessary in interpreting such data because the overlapping time courses of desensitization and whole-cell solution exchange may distort the peak current. We therefore estimated the EC_{50} values of muscimol, GABA, THIP, and β-alanine in outside-out patches in which solution exchange is much faster. Figure 2*C* shows ensemble average currents activated by maximal and half-maximal (i.e., peak current between 45 and 55%) agonist concentrations. The patch EC_{50} values spanned several orders of magnitude with the rank order being muscimol < GABA < THIP < β-alanine, identical to the rank order for the rate of patch current deactivation.

We estimated the microscopic unbinding rate (k_{off}) by fitting currents activated by pulses of the four agonists to a kinetic model of the $GABA_A$ receptor (Jones and Westbrook, 1995, 1996, 1997). The model (Fig. 3*A*) was first optimized to fit the responses to 5 and 505 msec pulses of GABA (10 mM). Thereafter, only k_{off} was allowed to vary as a free parameter in fitting currents activated by the other agonists. The optimum values of k_{off} were (in sec^{-1}) 40

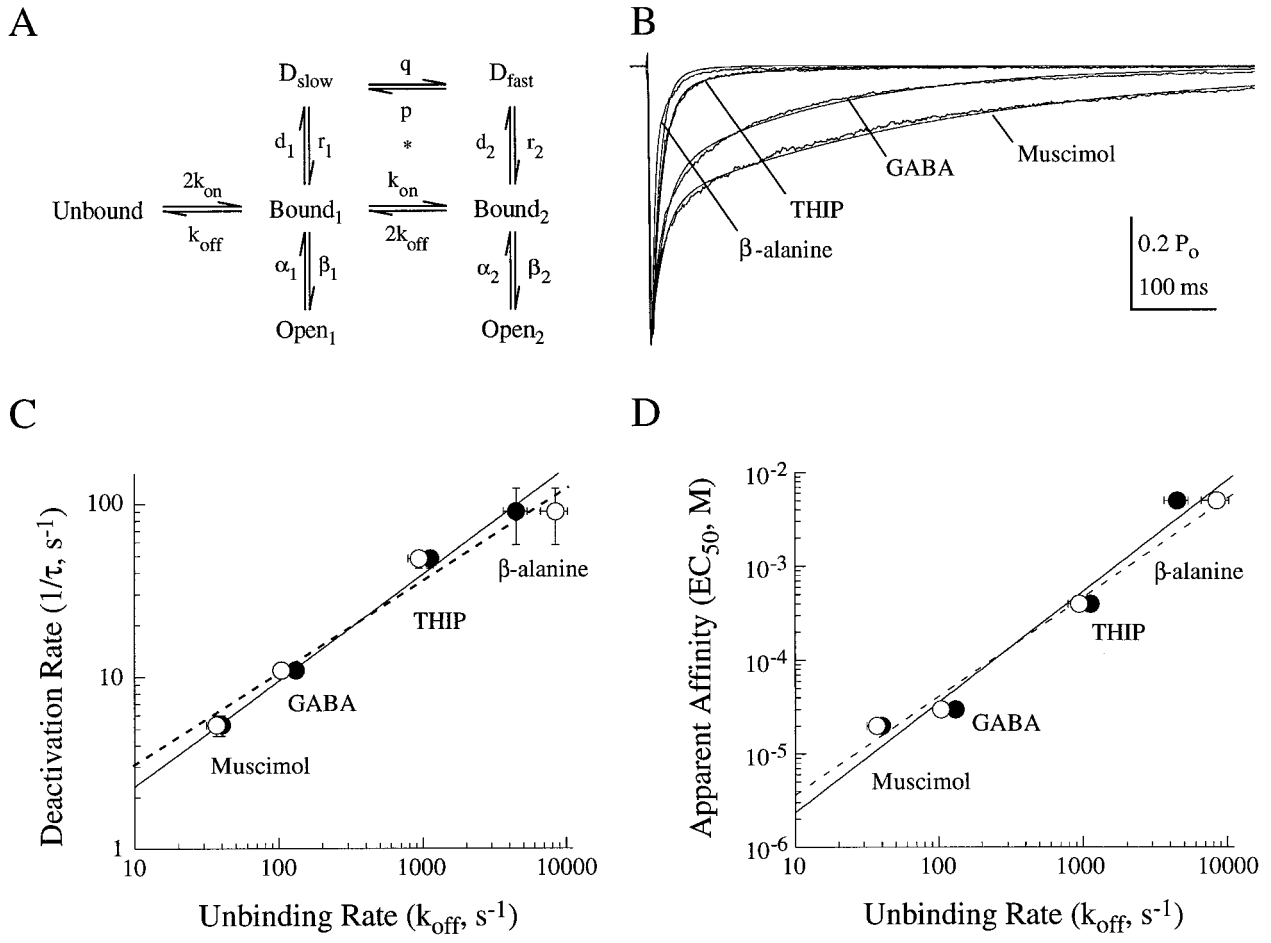

Figure 3. Agonist unbinding rates contribute to deactivation and affinity. *A*, A previously established kinetic model was modified and used to estimate the microscopic unbinding rate constants for different agonists. The development and performance of the model are described in detail in Jones and Westbrook (1995, 1997). *B*, Agonist-specific patch current deactivation (*noisy lines*) can be simulated (*smooth lines*) solely by changes in the unbinding rate. The model was optimized to fit 5 and 505 msec saturating GABA pulses and was then allowed to fit the deactivation phases for different agonists with only the unbinding rate (k_{off}) as a free parameter. Records were averaged, normalized to the same maximum open probability (P_o) (Jones and Westbrook, 1995, 1997), and aligned at the peak. The rates were (in sec^{-1}) $k_{on} = 5 \times 10^6$ M^{-1}, $\alpha_1 = 1100$, $\beta_1 = 200$, $\alpha_2 = 142$, $\beta_2 = 2500$, $d_1 = 13$, $r_1 = 0.2$, $d_2 = 1250$, $r_2 = 25$, $p = 2$, and $q = 10^{-2}$ M^{-1}. The *asterisk* denotes a net counterclockwise motion at steady state (see Materials and Methods). The best-fitting unbinding rates were (in sec^{-1}) 40 for muscimol, 131 for GABA, 1125 for THIP, and 4500 for β-alanine. *C*, *D*, The unbinding rate was closely correlated with both the patch-current deactivation rate (*C*) and the apparent affinity (*D*). Unbinding rates from fitting 5 msec (*closed circles* and *solid line*) and 505 msec (*open circles* and *dashed line*) pulse responses are shown with SEM bars for the *y*-axis and 95% confidence limits of the fit for the *x*-axis. In *C*, the *lines* are regression fits to the power function: $1/\tau = a k_{off}^{\ b}$, where *a* was 0.56 and *b* was 0.61 for 5 msec pulses and *a* was 0.90 and *b* was 0.53 for 505 msec pulses. In *D*, $EC_{50} = a k_{off}^{\ b}$, where *a* was 1.5×10^{-7} and *b* was 1.18 for 5 msec pulses and *a* was 3.2×10^{-7} and *b* was 1.05 for 505 msec pulses.

for muscimol, 131 for GABA, 1125 for THIP, and 4500 for β-alanine (Fig. 3*B*). Both the overall patch current deactivation rates [i.e., 1/(the weighted average of fast and slow components); Fig. 3*C*] and the EC_{50} values (Fig. 3*D*) were strongly correlated with k_{off}, suggesting that agonist unbinding kinetics are important in shaping the current as well as in determining the agonist selectivity. However, if diffusion-limited binding is assumed (Eq. 13), the expected microscopic affinity constants (Eq. 4) obtained using these unbinding rates were 4.3 nM for muscimol, 14 nM for GABA, 124 nM for THIP, and 490 nM for β-alanine, values more than a thousand times lower than the EC_{50} values observed experimentally (Fig. 2). These results imply that large differences in binding rate (k_{on}) between agonists contribute to agonist selectivity.

Comparison of GABA and β-alanine binding

As a direct test for differences in agonist binding rates, we set up a race for the binding site between agonists and a competitive antagonist. When an agonist and a competitive antagonist are rapidly and simultaneously applied to a patch, some channels will bind agonist and open, whereas others bind antagonist and become blocked. The resulting current (I_{race} = current with both ligands/current with agonist alone) depends on which ligand binds faster on average. We first used the antagonist SR-95531 (Hamann et al., 1988; Jones and Westbrook, 1997; Ueno et al., 1997) to determine whether or not GABA and β-alanine have similar binding rates. SR-95531 [K_N of 160 nM (Hamann et al., 1988)] meets the classical criteria for competitive antagonism in that it causes parallel right-shifts in the GABA concentration–response curve but evokes no response on its own. Its action is also modified by mutations in the putative GABA binding site (Ueno et al., 1997), suggesting that it interacts with the same regions occupied by GABA and other agonists. Coapplication of 1 mM SR-95531 and 1 mM GABA blocked 89 ± 2% ($n = 11$) of the peak current evoked by 1 mM GABA alone (Fig. 4*A*). Because no

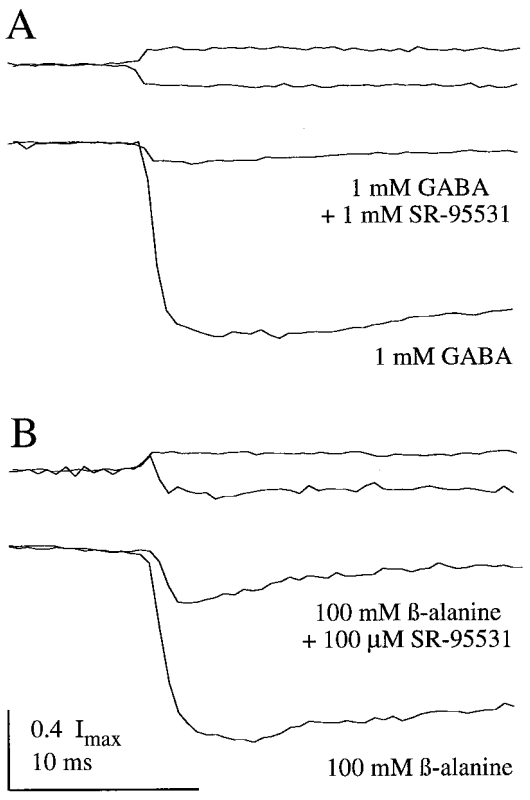

Figure 4. GABA and β-alanine bind at different rates relative to SR-95531. *A*, Simultaneous application of equal concentrations of GABA and SR-95531 activates 11% of the patch current evoked by GABA alone, suggesting that the antagonist occupied many receptors before GABA could bind. *B*, Simultaneous application of β-alanine at a concentration a thousand times higher than that of SR-95531 activates only 28% of the current evoked by β-alanine alone, suggesting that β-alanine binds much more slowly than GABA, relative to SR-95531.

current at all was observed when 1 mM SR-95531 was coapplied with 1 mM β-alanine, the concentration ratio was adjusted to favor β-alanine binding by a factor of 1000. Coapplication of 100 μM SR-95531 with 100 mM β-alanine blocked 66 ± 5% ($n = 3$) of the current evoked by 100 mM β-alanine alone (Fig. 4*B*). This result suggests that GABA and β-alanine have widely different binding rates and argues against diffusion-limited binding.

Binding and unbinding kinetics of the competitive antagonist SR-95531

The notion that agonist binding is not diffusion-limited is interesting because it implies that the mere physical proximity of ligand and receptor is not sufficient to produce binding but rather that some additional event must occur. The quantification of binding rates using race experiments might disclose the nature of such an event but requires knowledge of the antagonist kinetics. We therefore measured binding and unbinding rates for SR-95531. Figure 5 shows the method used to study equilibration of SR-95531 with the $GABA_A$ receptor. A saturating GABA pulse was applied as an assay of the maximum channel availability. The patch was then exposed to antagonist for a variable time interval, immediately after which the availability was measured again with a second GABA pulse (Fig. 5*A*,*B*). A plot of availability (i.e., the fraction of channels not blocked by antagonist) versus the duration of SR-95531 exposure confirms that both the rate and extent of block by SR-95531 depend on the antagonist concentration (Fig. 5*C*; four to six patches per concentration). After 400 msec, the availability had essentially reached steady state (see Eq. 3) and provides an estimate of the equilibrium block by SR-95531 in the absence of GABA. Therefore, a plot of the availability at 400 msec versus SR-95531 concentration (Fig. 6*A*) contains much the same information as that revealed by traditional dose–ratio methods (e.g., Schild analysis) but has the advantage that only a single agonist concentration is required. The data were described by a modified Hill equation (see Fig. 6 legend), in which N was constrained to be an integer. The best fit occurred with $N \cong 1$, yielding $K_N = K_n = 216$ nM, near the IC_{50} for block in Figure 6*A* and near to previously published values (Hamann et al., 1988; Ueno et al., 1997). These results confirm that the method is equivalent to the dose–ratio analysis used by Hamann et al. (1988) and suggest that there may be only a single functional antagonist binding site (see below), although there are more complicated interpretations.

The macroscopic affinity constant K_N is a function of the microscopic binding and unbinding rates as well as the number of binding sites (Eqs. 4–7). These same factors determine the time course of the blocking relaxation (see Fig. 5*C*) and can therefore be extracted from it using Equation 8. A microscopic equilibration time constant τ_n was first derived by fitting the data of Figure 5*C* to an exponential relaxation equation (see Eqs. 2, 9). Plotting $1/\tau_n$ versus the concentration of SR-95531 yields a different straight line for each value of N, the slopes of which are k_{on} and which cross the y-axis at k_{off} (Fig. 6*B*). To determine further which combination of N, k_{on}, and k_{off} is most accurate, we directly and independently measured the SR-95531 unbinding time course (Fig. 7) (Jones and Westbrook, 1997). Patches were pretreated with a saturating concentration (10 μM) of SR-95531, and the fraction of available channels was tested with a saturating GABA pulse at increasing intervals after removal of the antagonist. As the unbinding interval was increased, larger currents could be evoked by the GABA pulse (Fig. 7*A*). This unbinding time course was fit to an exponential relaxation equation (see Eqs. 2, 9), yielding microscopic unbinding time constants (τ_n) of 110, 61, and 47 msec for $N = 1$, 2, and 3 (Fig. 7*B*). If there is more than one antagonist binding site and occupancy of any one site is sufficient to block the receptor, then the unbinding time course should be sigmoidal as shown by the fits for $N = 2$ and 3. However, the best fit to the data was obtained with $N = 1$, yielding a microscopic unbinding rate ($k_{off} = 1/\tau_n$) of 9.1 sec^{-1}. The calculated microscopic affinity constant ($K_n = K_N = k_{off}/k_{on}$, where $k_{on} = 4.28 \times 10^7$ M^{-1} sec^{-1} for $N = 1$ from Fig. 6*B*) was thus 213 nM, indistinguishable from the value obtained in Figure 6*A*. These results demonstrate that our estimates of kinetic parameters and the number of binding sites derived from separate analyses of the onset, steady-state, and offset kinetics of SR-95531 are in excellent agreement.

Binding rates are agonist-specific and are not limited by diffusion

Having established the antagonist binding rate, we used race experiments to measure the agonist binding rates (Eq. 12). Race experiments between SR-95531 and muscimol, GABA, THIP, and β-alanine are illustrated in Figure 8*A*. Coapplication of the antagonist always produced smaller currents than did the agonist alone. For muscimol and GABA, equal concentrations (1 mM) of agonist and antagonist were used. For the other two agonists, the ligand concentration ratios (agonist/SR-95531) were adjusted to favor the agonist (THIP, 30 mM/200 μM; β-alanine, 100 mM/100

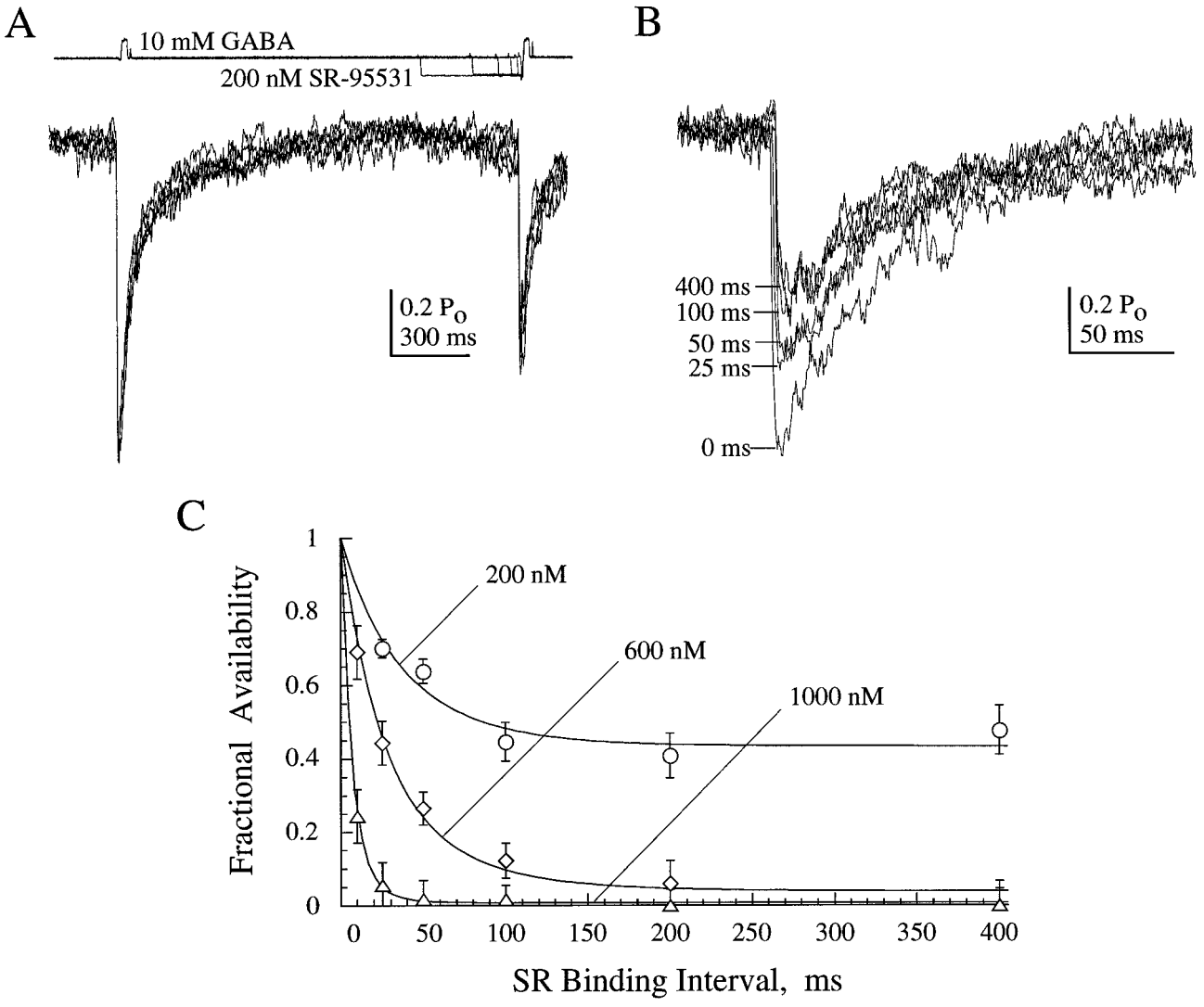

Figure 5. The concentration and time dependence of block by SR-95531. *A*, The equilibration time course of SR-95531 in the absence of GABA was measured in outside-out patches. The *top traces* are the liquid junction currents measured at the open pipette tip after the experiment. After a brief pulse of saturating GABA to assay the channel availability, the patch was exposed to SR-95531 for a variable interval after which channel availability was assayed with a second GABA test pulse. *B*, The response to the test pulse from *A*, on an expanded time scale, shows that channel availability declined with increasing durations of SR-95531 exposure. *C*, Plots of channel availability versus the duration of SR-95531 exposure reveal that the rate and extent of block increase with antagonist concentration. The data for each concentration were fit to the equation: Availability = $(1 - [P_{n\infty} - (P_{n\infty} - P_{n0})e^{-t/\tau}])^N$ (see Eqs. 2, 9), with P_{n0} constrained to 1 and N constrained to be an integer. The parameters $P_{n\infty}$ and τ contain information about the microscopic binding and unbinding rates (see Fig. 6). In this and all subsequent figures, the pooled data have been corrected for any unbinding of SR-95531 that occurs during the agonist pulse according to the equation: $I_{corr} = (F_{err} - I_{obs}) / (F_{err} - 1)$. I_{corr} is the corrected current, I_{obs} is the observed current, and F_{err} is the fractional unbinding that would occur over the length of the agonist pulse if all channels were initially bound with antagonist (see Fig. 7).

μM) because currents were difficult to detect when concentrations were equal. The agonist binding rates calculated from the measured values of I_{race}, the known ligand concentrations, and the binding rate of SR-95531 measured in the previous section are shown in Figure 8*B*. Also shown is the predicted binding rate constant for a diffusion-limited process (k_{diff}; Eq. 13). The binding rates were (in M^{-1} sec^{-1}) 9.1 ($\times 10^9$) for diffusion, 4.28 ± 0.8 ($\times 10^7$) for SR-95531 (n = 4–6), 5.38 ± 0.8 ($\times 10^6$) for GABA (n = 11), 4.74 ± 0.6 ($\times 10^6$) for muscimol (n = 4), 4.57 ± 0.2 ($\times 10^5$) for THIP (n = 3), and 2.25 ± 0.2 ($\times 10^4$) for β-alanine (n = 3). Therefore the binding rates were two to five orders of magnitude slower than was that of a diffusion-limited process. To ensure that using unequal agonist and antagonist concentrations did not yield artificially slow binding rates, we also raced 1 mM THIP against 1 mM SR-95531 and 10 mM β-alanine against 100 μM SR-95531. In these experiments, the calculated binding rates were (in M^{-1} sec^{-1}) 9.55 ± 0.6 ($\times 10^5$) for THIP (n = 2) and 3.22 ± 0.9 ($\times 10^4$) for β-alanine (n = 3), demonstrating that changing the (agonist/antagonist) concentration ratio by a factor of 150 altered the binding rate estimate only by a factor of two, a negligible difference in comparison with the wide range of binding rates.

Binding energetics critically determine the affinity of the $GABA_A$ receptor

The two major theories of chemical reaction kinetics, collision theory and Eyring's transition state theory, both use the concept of activation energy (E_a) to account for the rate constant of a

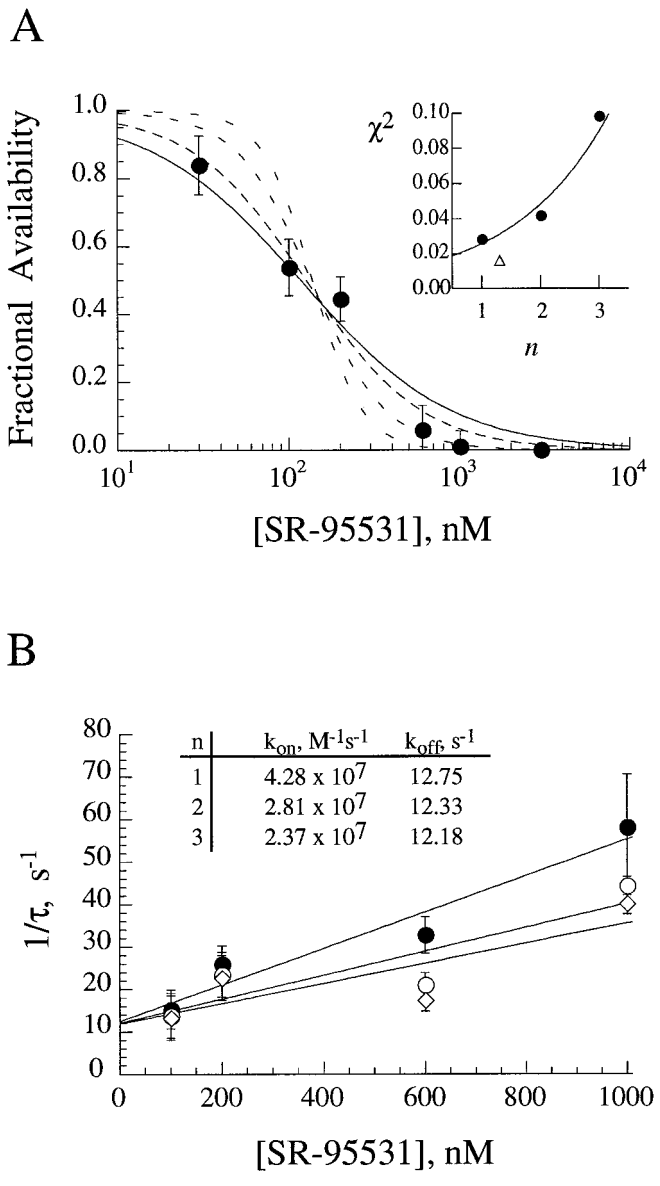

Figure 6. SR-95531 appears to bind at a single site. *A*, The block at steady state (*filled circles*) from Figure 5 is plotted here versus SR-95531 concentration and suggests a single antagonist binding site. The data were fit to the normalized Hill equation: $I/I_{max} = 1 - [1/(K_H/[A]^N + 1)]$, in which N could be constrained to be an integer (*solid line*, $N = 1$; *dashed lines*, $N = 2$, 3, or unconstrained). The best fit occurred with $N \cong 1$, yielding $K_N = K_n = 216$ nM. The *inset* shows the increasing error of the fit (χ^2) as the assumed number of binding sites departs from 1. The *circles* are with N constrained, whereas the *triangle* is with N as a free parameter and occurs near $N = 1$. *B*, To extract k_{on} and k_{off} from the onset time course of SR-95531 block (Fig. 5*C*), we plotted the reciprocal of the fitted time constant $1/\tau$ versus the SR-95531 concentration, for fits in which N was constrained to be 1 (*filled circles*), 2 (*open circles*), or 3 (*diamonds*). These plots yield straight lines with slope equal to k_{on} and intercept equal to k_{off} (Eq. 8). The table of the best fit values (*inset*) shows that the estimates of k_{on} and k_{off} vary less than twofold between one and three assumed sites.

reaction (Wentworth and Ladner, 1972; Freifelder, 1982). The reactants (e.g., unbound ligand and receptor) and the products (e.g., the bound receptor) are viewed as being separated by an energy barrier. Only that fraction of encounters between ligand and receptor possessing sufficient energy will result in binding. If the height of the barrier is zero, then all encounters will lead to binding, and the rate will be limited by the rate of diffusion of ligand into the binding site. We therefore used the deviation from diffusion-limited binding to calculate the activation energy of ligand binding from the Arrhenius equation (Fig. 8*C*; Eq. 14). The activation energies were (in kcal M^{-1}) 3.2 ± 0.6 for SR-95531, 4.4 ± 0.6 for GABA, 4.5 ± 0.6 for muscimol, 5.8 ± 0.3 for THIP, and 7.6 ± 0.7 for β-alanine.

Figure 9*A* illustrates the correlation between the microscopic rates k_{diff}, k_{on}, and k_{off} and the macroscopic EC_{50} values for the ligands tested. The unbinding rate increased with increasing EC_{50} as shown in Figure 3*D*, whereas the binding rate decreased with increasing EC_{50} and departed entirely from the rate expected for diffusion. The correlation between k_{on} and EC_{50} was steeper than that for k_{off}, demonstrating that binding kinetics contribute more than unbinding to determining selectivity.

The close correspondence between binding kinetics and affinity can be attributed primarily to the height of the activation energy barrier. Figure 9*B* shows that two separately derived estimates of affinity, the directly measured macroscopic EC_{50} values (*triangles*) and the ratio of microscopic rate constants k_{off}/k_{on} (*circles*) estimated kinetically, were correlated with activation energy and were similar to each other. As expected, the macroscopic measurements deviate somewhat from the microscopic values for low-affinity agonists because, as the unbinding rates increase, the gating steps become rate limiting in determining the apparent affinity. Neither the microscopic nor macroscopic affinities were compatible with those predicted for diffusion-limited binding (*squares* on *y*-axis). These results have two important implications. First, the similarity between macroscopic measurements and microscopic estimates shown in Figure 9*B* suggests that the simplifying assumptions we made (see Materials and Methods) were reasonable approximations. Second, the fitted line through the microscopic affinities in Figure 9*B* intersects the *y*-axis at 15 pM, which would therefore be the microscopic affinity constant for a hypothetical ligand with diffusion-limited binding (i.e., requiring zero activation energy). This value is a theoretical maximum limit for any agonist at the $GABA_A$ receptor, assuming that binding occurs via the same reversible mechanism as that studied here. All known ligands have much lower affinities, suggesting that none bind in a diffusion-limited manner.

The energetics of binding, unbinding, and affinity are summarized in Figure 9*C*. Each *thick dark line* can be viewed as the energy barrier diagram for one ligand (cf. Wentworth and Ladner, 1972; Freifelder, 1982). The reaction coordinate axis is an as yet unspecified measure of progress from unbound to bound (see Discussion). The hypothetical diffusion-limited ligand faces no energy barrier as binding progresses (from I to II) and binds rapidly. However, this ligand must climb out of a deep energy well to unbind and thus unbinds slowly. Such a ligand would have maximal affinity. As ligand affinity decreases (from I to III), the height of the barrier increases (from II to IV), and the energy depth of the bound state decreases, reducing the deactivation energy (E_d). This energy surface therefore accounts for the correlation between binding and unbinding rates and provides an empirical explanation for the ligand selectivity of the receptor. The deactivation energies were (in kcal M^{-1}) 13.8 for diffusion, 12.3 for SR-95531, 10.7 for GABA, 11.4 for muscimol, 9.4 for THIP, and 8.6 for β-alanine. Finally, for each ligand the total energy difference between the unbound and bound states defines the equilibrium affinity constant by the relation: $E_{tot} = E_a - E_d = RT\ln(k_{off}/k_{on})$. The total energy differences were (in kcal M^{-1})

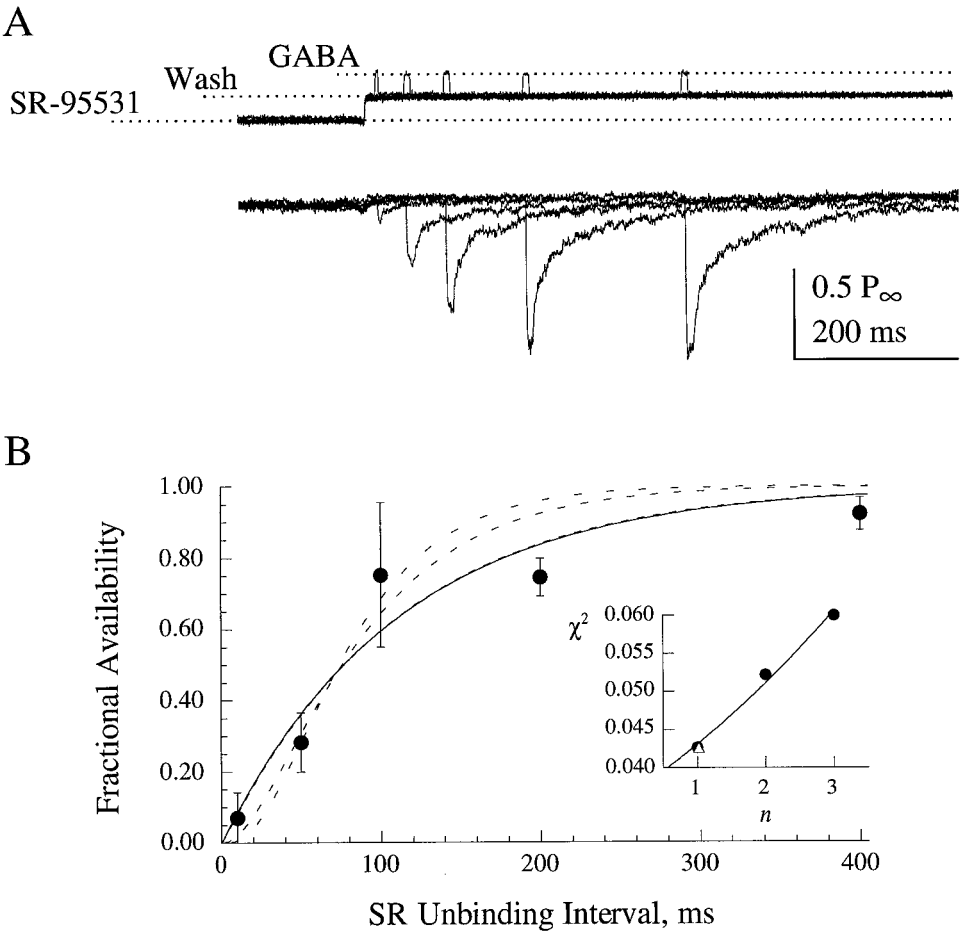

Figure 7. Direct measurement of the SR-95531 unbinding rate. *A*, The SR-95531 unbinding time course was measured directly by pre-equilibrating a patch in a saturating antagonist concentration (10 μM) and measuring the channel availability with saturating (10 mM) GABA pulses at a variable interval after antagonist removal. The *top traces* are the open tip currents. The *lower traces* show the increasing channel availability at increasing intervals after SR-95531 is removed. *B*, A plot of availability versus the SR-95531 unbinding interval was fit to the same equation given in the legend to Figure 5*C*, with P_{n0} constrained to 0, $P_{n\infty}$ constrained to 1, and N unconstrained or constrained to be an integer. The *solid line* is the fit for $N = 1$. Values of $N > 1$ produce a sigmoidal rising phase (*dashed lines*) because multiple antagonist molecules would need to unbind before the channel becomes available. However, the error of the fit increased as the number of sites assumed departed from 1 (*inset*; *filled circles*). The *triangle* represents the fit with N unconstrained, which occurred with N essentially equal to 1 and yielded an unbinding rate of $k_{off} = 1/\tau = 9.1\ sec^{-1}$, near the value obtained in Figure 6.

13.8 for diffusion, 9.1 for SR-95531, 6.3 for GABA, 6.9 for muscimol, 3.6 for THIP, and 1.0 for β-alanine.

DISCUSSION

We examined the contributions of the microscopic binding and unbinding transitions to the affinity of ligands at the $GABA_A$ receptor. Unbinding is a major determinant of the deactivation time course after brief GABA pulses such as are likely to occur at the synapse. However, binding was much slower than expected for a diffusion-limited process, suggesting that a significant energy barrier limits the fraction of encounters between the ligand and receptor that result in channel activation. The height of this barrier is ligand-specific and can thus account for ligand selectivity.

Validity of the initial assumptions

Our findings contrast with the widespread view that ligand binding is diffusion-limited and that affinity is primarily determined by the unbinding rate. However, the few studies that have directly compared microscopic binding rates between different ligands at nACh (Sine and Steinbach, 1986; Papke et al., 1988; Zhang et al., 1995; Akk and Auerbach, 1996) or glutamate receptors (Benveniste et al., 1990b; Benveniste and Mayer, 1991) have found these rates to be at least slightly ligand-dependent. In particular, Zhang et al. (1995) concluded that affinities for several nACh receptor ligands were primarily determined by nondiffusion-limited binding. We used ligands spanning a large range of affinities, which allowed a systematic treatment of correlations between ligand kinetics, selectivity, and structure.

We interpreted the kinetics of SR-95531 blocking and unblocking in microscopic terms under the assumption that this antagonist prevents gating. However, SR-95531 and bicuculline noncompetitively inhibit currents activated by general anesthetics (Ueno et al., 1997), suggesting that channel gating occurs with antagonist bound under certain conditions. If the channel can desensitize with antagonist bound, then our estimates of SR-95531 kinetics actually reflect macroscopic processes. This scenario is unlikely, however, because some treatments that increase macroscopic desensitization [e.g., inhibition of calcineurin (Jones and Westbrook, 1997)] also speed the unblocking of SR-95531, opposite to what is expected if the unblocking time course involves desensitized states.

Our kinetic estimates also depend on the number and cooperativity of binding sites. Interestingly, the best fits occurred with only one SR-95531 site despite the presence of at least two agonist sites (Constanti, 1977a,b; Macdonald et al., 1989; Twyman et al., 1990), suggesting that only one of these sites can bind antagonist. This idea is consistent with Hill coefficients close to unity observed by others for SR-95531 and bicuculline (Ueno et al., 1997; Jonas et al., 1998) and with reports of nonequivalent agonist binding sites on many receptors (Dionne et al., 1978; Sine and Steinbach, 1986; Colquhoun and Ogden, 1988; Jackson, 1989; Raman and Trussell, 1995; Sine et al., 1995; Akk et al., 1996; Lavoie and Twyman, 1996; Lavoie et al., 1997; Clements et al., 1998). The possibility remains that we could not detect multiple antagonist sites because of limited time resolution or because the sites are so unequal that only one is rate limiting. However, the

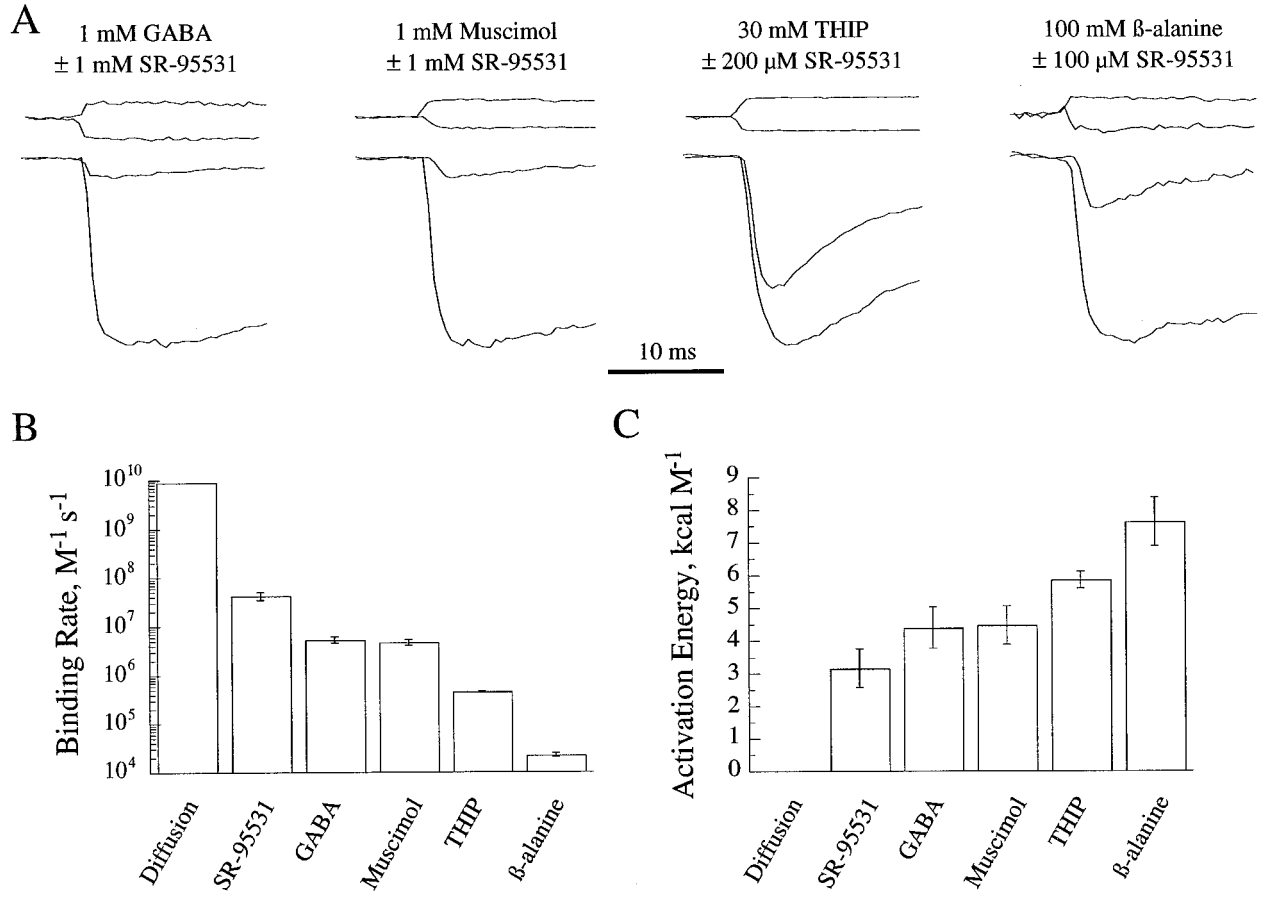

Figure 8. Agonist binding rates are limited by an activation energy barrier. *A*, Agonist binding rates were measured by examining the instantaneous competition between agonists and SR-95531. Applications of agonist alone and agonist plus SR-95531 were alternated on the same patch, and responses for each condition were averaged. The *top traces* are the open tip currents. *B*, Agonist binding rates were calculated from the ratio of peak currents in the presence and absence of antagonist (Eq. 12). The rate for SR-95531 is from Figure 6*B* for $N = 1$, and the rate for a hypothetical agonist with diffusion-limited binding was calculated from Equation 13. All ligands tested had binding rates orders of magnitude slower than diffusion, and these rates were strongly agonist-specific. *C*, The ratio of ligand binding rates to the diffusion-limited rate was used to calculate the height of an activation energy barrier between the unbound and bound states using the Arrhenius equation (Eq. 14). As the height of this barrier increases, the binding rate decreases.

estimated binding rate of SR-95531 changed less than twofold whether assuming one or three sites. Therefore, errors in SR-95531 measurements would cause proportional errors in agonist binding rate estimates but would not qualitatively alter our conclusions.

Physical properties governing selectivity

Despite remarkable biochemical and molecular advances in understanding receptor structure, there is still insufficient information for a detailed structural picture of binding or gating. A complementary approach is to generate highly simplified structural models of the binding site with dynamics that reproduce the kinetics of ligand selectivity. For the $GABA_A$ receptor, these kinetics can be summarized by the energy surface in Figure 9*C*, which is a function of two nonstructural parameters: affinity and a reaction coordinate. What structural correlates might be assigned to these parameters to yield a plausible binding-site model?

Ligand chemistry, conformational flexibility, and orientation may all affect interactions with the receptor. None of these, however, can account for the kinetics we observed. For example, GABA and β-alanine have similar chemistry and flexibility (Fig. 10*A*) but are near opposite ends of the kinetic spectrum. Furthermore, the speed of reorientation is inversely related to size (Lauffer, 1989), yet the smallest ligand, β-alanine, binds most slowly. In contrast, the excellent correlation between affinity and the "length" of the GABA-like region of each ligand (Fig. 10*B*) strongly suggests a length-based selectivity mechanism (Chambon et al., 1985).

The reaction coordinate is a common, often qualitative, metric of the progress of a reaction. Formally, it is the steepest path along an energy hypersurface connecting the reactants and products that passes through the transition state (Eyring, 1935; Marcus, 1964). For length-based selection, an appropriate reaction coordinate is the physical distance between the ligand and the groups comprising the binding site.

Finally, an energy barrier implies an uncomfortable region between the unbound and bound states. Such a region might exist, for example, if the ligand must lose waters of hydration or the binding site must change shape before binding can occur. Similar hypotheses have been considered for the nACh receptor (Zhang et al., 1995). We simulated our observations using both scenarios.

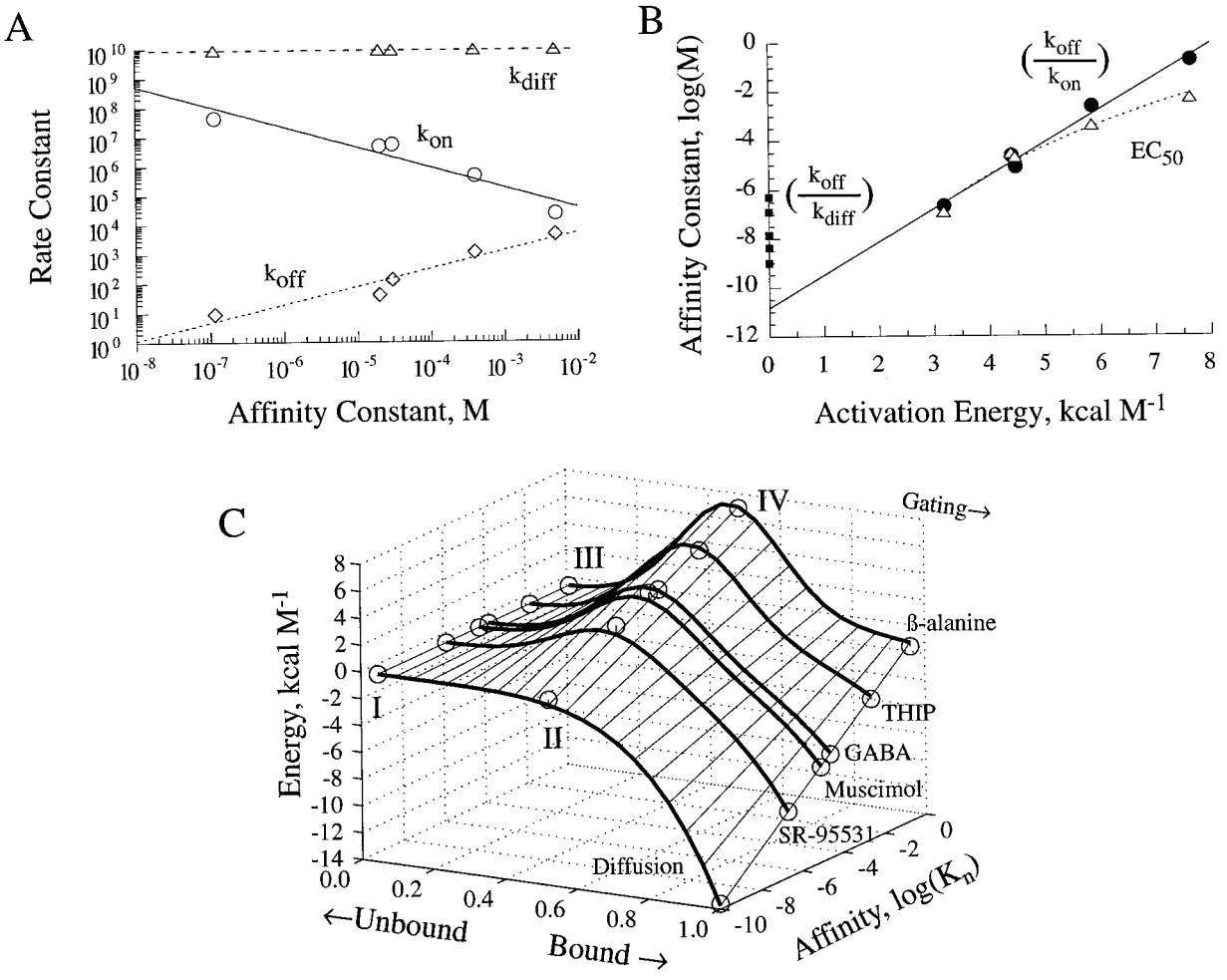

Figure 9. The energy barrier between unbound and bound states defines affinity and deactivation kinetics. *A*, A plot of the predicted diffusion-limited binding rate and the actual binding and unbinding rates versus the affinity constant reveals that differences in affinity between ligands are related to differences in both binding and unbinding. However, binding rates were more steeply correlated with affinity than were unbinding rates. The *lines* are regression fits to the power function: $k = aC_{50}{}^{b}$, where a was 1528 and b was -0.69 for k_{on}, a was 84786 and b was 0.61 for k_{off}, and a was 9.1×10^9 and b was 0 for k_{diff}. *B*, The directly measured macroscopic EC_{50} values (*triangles*) (IC_{50} for the antagonist) and the kinetically estimated microscopic affinity constants (*circles*) both increase with the height of the energy barrier between the unbound and bound states. The deviation between the two curves is expected because unbinding rates are faster for lower microscopic affinities, allowing gating steps to become rate limiting in determining the macroscopic EC_{50}. The *small squares* on the *y*-axis are the affinities predicted for the measured unbinding rates if diffusion-limited binding is assumed. The *solid line* is the linear regression to the microscopic values, with a slope of 1.3 and an intercept of -10.8, suggesting a theoretical maximum limit for $GABA_A$ receptor affinity of 15 pM. *C*, Both affinity and kinetics can be understood in terms of an energy barrier between the unbound and bound states. The energy of the ligand-receptor system is plotted as a function of affinity and a reaction coordinate that measures the progress of the binding (or unbinding) reaction. As a ligand undergoes binding, it travels along an energy surface from *left* to *right* (*thick dark lines*). A diffusion-limited ligand faces no energy barrier to binding (from I to II) but faces a large barrier in the reverse direction. Such a ligand would bind quickly, unbind slowly, and thus have the highest possible affinity. Lower affinity agonists such as β-alanine face a larger energy barrier to binding (from III to IV) but a smaller barrier to unbinding. The *solid lines* describe an empirically chosen surface fitted to the data: Energy $= a(EC_{50} + 0.2)(bF^6)(0.5 + F^2)^{-1} + (EC_{50} + 10)(c^{-0.2^{-2}(F - 0.5)^2})$, where F is the fractional progress from unbound to bound and a, b, and c are fitting constants. All energies are with reference to that of the unbound state (0 kcal M^{-1}), and the transition state is arbitrarily placed halfway through the reaction.

Here, we present only the latter because it provides a natural link between binding and channel gating.

A flexible binding-site model

We treated the agonist as a pair of particles separated by a fixed length and the binding site as another set of particles. The energy of interaction between any two particles varies nonlinearly with distance (see Materials and Methods). The energy profile for each agonist is thus the changing energy of the system as the agonist and the binding site are brought together. The binding site behaves as a pair of mobile "arms" attached to fixed "anchor" sites by spring-like tethers (Fig. 11*A*). The anchors are separated by a length (L_{site}), and the arms rest in the energy wells created by the anchors (Fig. 11*B*). Binding occurs when the agonist falls into the secondary energy wells created by the arms. Binding is diffusion-limited only if the agonist is long enough to span the distance between these wells. Shorter agonists bind more slowly because the arms must move to accommodate them, which requires activation energy. In addition, because the arms are displaced from rest, the

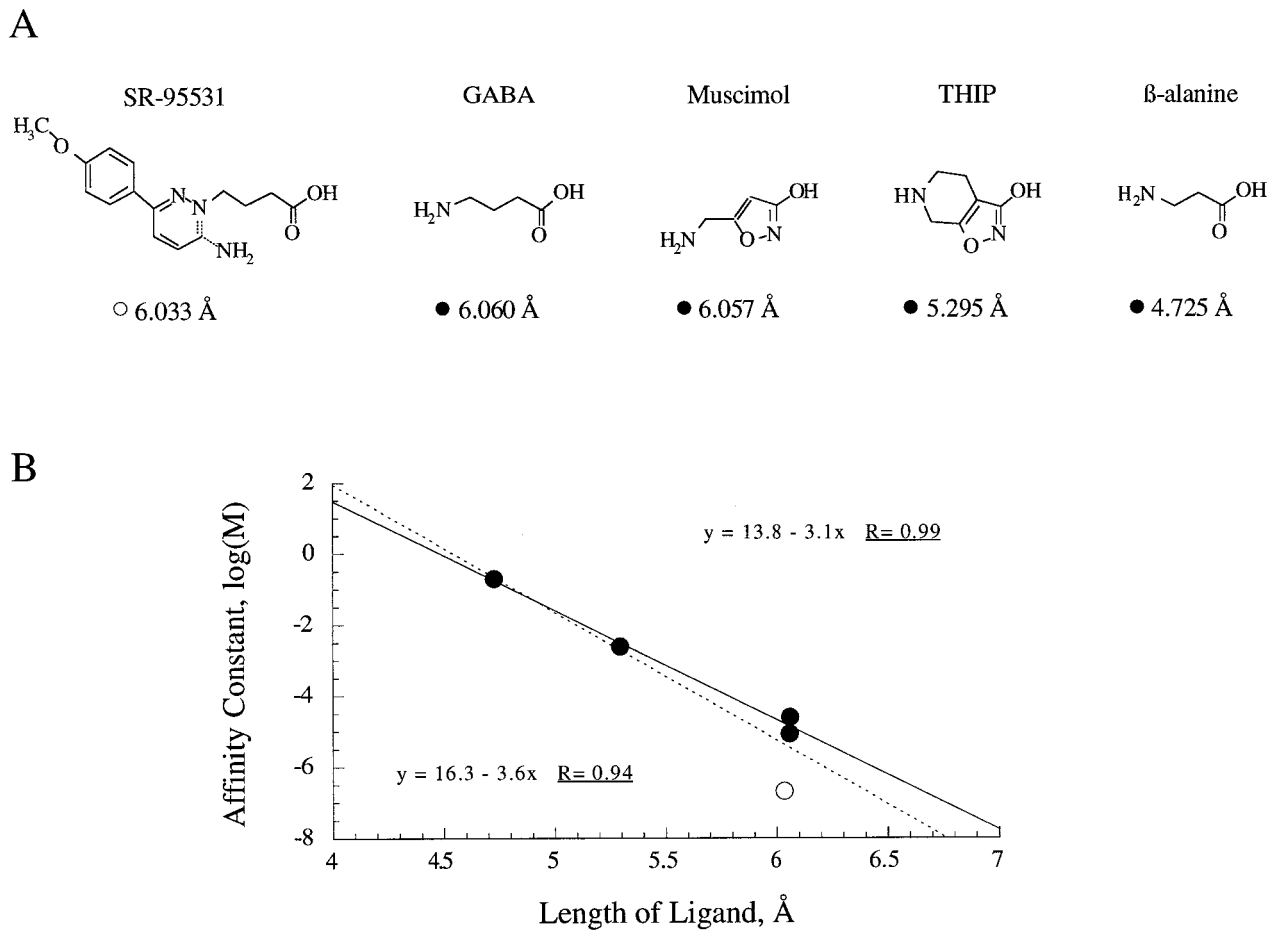

Figure 10. Affinity is correlated with ligand length. *A*, The chemical structures of the ligands used in our experiments are arranged in order of decreasing binding rate from *left* to *right*. For each ligand, the length of the GABA-like region is given below the structure (as measured from the nitrogen to the hydroxyl oxygen in the most energetically favorable conformation; see Materials and Methods). *B*, A plot of ligand affinity [i.e., $\log(K_n)$] versus the length of the GABA-like region reveals a strong linear correlation, suggesting a length-based selectivity mechanism for the GABA binding site. The *upper equation* (*solid line*) is the regression for the four agonists. The *lower equation* (*dashed line*) is the regression for all five ligands.

energy of the bound state is higher and unbinding is faster than for long agonists. The kinetics and selectivity resulting from this model closely match those observed experimentally (Fig. 11*C*).

We interpret the well depths and radii of the model as the average local environment experienced by the ligand and not as descriptions of specific amino acid residues, although the latter is also possible. The model predicts that both binding and unbinding depend on receptor structure rather than on diffusion, involving energies on the scale of a few van der Waals or hydrogen bonds (Morris et al., 1996). The model also explicitly requires the ligand to perform thermodynamic work (approximately the activation energy) on the receptor by moving the arms away from rest, and this movement could be coupled to gating. The receptor expends compensatory work (approximately the deactivation energy) to stabilize the ligand. Our data suggest that the binding of two GABA molecules can perform enough work (~12 kcal M^{-1}) to drive a coupled gating reaction from 0.01 to 99.99% completion (Freifelder, 1982). We cannot yet say how much of this work is actually used to drive gating, whether it is conserved, or how it is distributed among enthalpic and entropic components (Maksay, 1994). Nonetheless, such a mechanism implies that only nondiffusion-limited ligands can be agonists because otherwise they cause no movement of the receptor.

Because ligand chemistry was ignored, it is unsurprising that the model fails to predict the fast binding and slow unbinding of the antagonist SR-95531. Many $GABA_A$ receptor antagonists contain aromatic rings (Chambon et al., 1985; Hamann et al., 1988; Huang and Johnston, 1990) that may tether the ligand near the binding site. Such tethering could simultaneously enhance the probability of binding, slow unbinding, and interfere with movements involved in the coupling of binding to gating. Finally, muscimol is slightly shorter than GABA but unbinds more slowly. Perhaps GABA can twist and shorten while in the binding site, leading to premature unbinding, whereas muscimol cannot because of its conformational restriction.

Multiple protein domains affect the apparent affinity of many receptors (Stern-Bach et al., 1994; Smith and Olsen, 1995). For example, in $GABA_A$, glycine, and nACh receptors, discontinuous segments including aromatic residues appear to come together to form a binding pocket (Dennis et al., 1988; Schmieden et al., 1992, 1993; Vandenberg et al., 1992; Amin and Weiss, 1993). Furthermore, mutations that alter these regions by as little as a single hydroxyl group dramatically alter the EC_{50} (Amin and Weiss, 1993; Schmieden et al., 1993). Our model is compatible with these findings in that (1) successful binding involves the coordinated motion of separate parts of the receptor and (2) variations of a fraction of an angstrom or a single hydrogen bond cause quite large changes in affinity. Such small structural effects

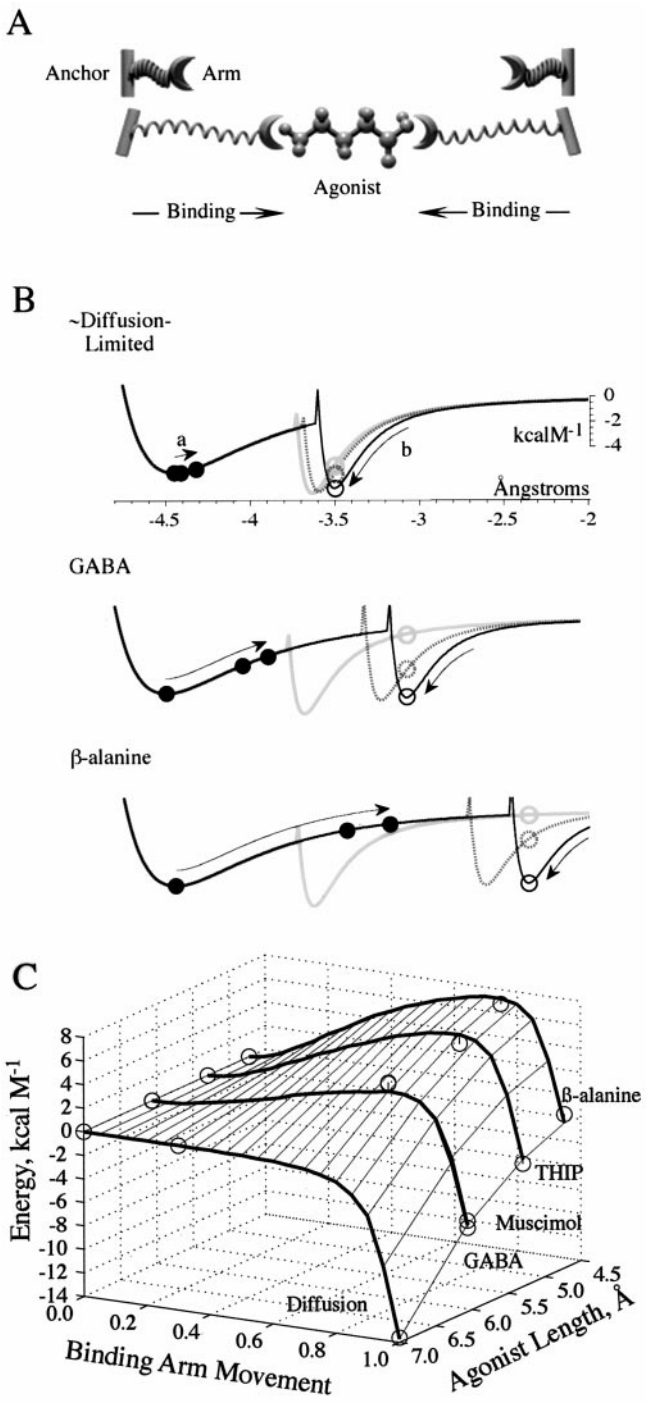

Figure 11. A flexible binding-site model can account for agonist selectivity. *A*, A flexible binding site can be envisioned as a pair of binding arms anchored to the rest of the protein by spring-like tethers. At rest, the arms are widely spaced (*top*), whereas they must move closer together to secure an agonist within the binding site (*bottom*). This movement requires energy, symbolized by stretching the springs. *B*, A flexible-site model was implemented by calculating the profile of energy wells from the Lennard–Jones equation (see Materials and Methods) for interactions between three kinds of particle: the anchors (out of view to the *left* and *right*), the movable arms (*filled circles*), and the agonist endpoints (*open circles*). The *y*-axis measures the energy experienced by each particle. The *x*-axis measures the distance from the center of the binding site. Only the *left half* of the symmetrical system is shown here, and for clarity the repulsive energy components are not displayed. Simulations were initialized with the arm particle resting in the well generated by the anchor (at −4.4 Å). The arm itself generates a secondary well (the *gray* well at −3.65Å) that will bind the agonist. The agonist is centered in the binding site but is not secured at the bottom of a well in the unbound state (one endpoint is shown by the *gray circles*; the other is out of view to the *right*). As binding proceeds, the arm moves closer to the agonist (*arrow* at *a*), which requires energy because it involves climbing out of a well. The highest energy occurs partway through the movement, when neither the arm nor the agonist are in a well (i.e., the transition state, *stippled lines* and *circles*). Binding is complete when the agonist falls to the bottom of the well generated by the approaching arm (*arrow* at *b*, *black lines* and *circles*). The reaction energy can be divided approximately into activation energy expended by the agonist in lifting the arm from its rest level and deactivation energy gained by the agonist as it sinks into the binding well. The difference between these energies is exponentially related to the probability that the agonist will be found in the bound state and thus determines affinity. *C*, The graph shows the energy surface predicted by the model to account for the kinetics of agonist selectivity and is thus a reinterpretation of the kinetic data of Figure 9*C* in structural terms. The progress of the reaction is represented here by the fractional arm movement [multiply by (3.6 Å − 0.5 × agonist length) for the actual movement], and the agonist length has been substituted for the affinity constant. The model was optimized by iteratively varying the site length L_{site}, the well depths ϵ, and the well radii r_{eqm} to minimize the error between the experimental data (*circles*) and the model prediction (*solid lines*). The best-fitting parameters gave excellent agreement with the experimental data (root mean-squared error = 0.41 kcal M^{-1}) and were L_{site} = 14.2 Å; r_{eqm} = 2.65 Å and ϵ = 6.04 kcal M^{-1} for the anchors; and r_{eqm} = 0.82 Å and ϵ = 5.50 kcal M^{-1} for the arms (~7.2 Å between arm energy wells at rest). Note that unlike the empirical surface used in Figure 9*C*, the curvature and position of barrier peaks for this theoretical surface vary with agonist length.

may arise physiologically via subunit differences or movements propagated through the protein because of interactions with the cytoskeleton or phosphorylation (e.g., Jones and Westbrook, 1997).

Implications for synaptic transmission

We studied responses evoked by different agonists at the same receptor. However, at GABAergic synapses the agonist is always the same, whereas the receptor subtypes may differ. Because deactivation is strongly influenced by the rate of agonist unbinding, some of the observed variation in IPSC duration probably results from differences in unbinding between receptor subtypes because of differing subunit compositions or regulation (Puia et al., 1994; Verdoorn, 1994; Tia et al., 1996; Auger and Marty, 1997; Jones and Westbrook, 1997). If binding rates depend on receptor structure, as in the flexible site model, then the correlations between binding, unbinding, and affinity suggest that receptors mediating rapidly decaying IPSCs may be less efficient at binding GABA than are those mediating long-lasting IPSCs. Binding efficiency is critical at low GABA concentrations, such as may occur during "spillover" (Isaacson et al., 1993; Nusser et al., 1997) or "cross talk" (Barbour and Häusser, 1997). Thus, neurons with fast IPSCs may be less sensitive to these modes of inhibition. Even in situations in which the concentration is high, different binding rates will result in different degrees of occupancy if the GABA transient is brief (Clements et al., 1992; Frerking and Wilson, 1996; Auger and Marty, 1997; Diamond and Jahr, 1997; Galarreta and Hestrin, 1997; Perrais and Ropert, 1997). Receptors underlying fast IPSCs may thus have a lower occupancy than those underlying slow IPSCs.

REFERENCES

Akk G, Auerbach A (1996) Inorganic, monovalent cations compete with agonists for the transmitter binding site of nicotinic acetylcholine receptors. Biophys J 70:2652–2658.

Akk G, Sine S, Auerbach A (1996) Binding sites contribute unequally to the gating of mouse nicotinic αD200N acetylcholine receptors. J Physiol (Lond) 496:185–196.

Amin J, Weiss DS (1993) $GABA_A$ receptor needs two homologous domains of the β-subunit for activation by GABA but not by pentobarbital. Nature 366:565–569.

Auerbach A (1993) A statistical analysis of acetylcholine receptor activation in *Xenopus* myocytes: stepwise versus concerted models of gating. J Physiol (Lond) 461:339–378.

Auger C, Marty A (1997) Heterogeneity of functional synaptic parameters among single release sites. Neuron 19:139–150.

Barbour B, Häusser M (1997) Intersynaptic diffusion of neurotransmitter. Trends Neurosci 20:377–384.

Benveniste M, Mayer ML (1991) Kinetic analysis of antagonist action at *N*-methyl-D-aspartic acid receptors. Biophys J 59:560–573.

Benveniste M, Clements J, Vyklicky Jr L, Mayer ML (1990a) A kinetic analysis of the modulation of *N*-methyl-D-aspartic acid receptors by glycine in mouse cultured hippocampal neurons. J Physiol (Lond) 428:333–357.

Benveniste M, Mienville J-M, Sernagor E, Mayer ML (1990b) Concentration-jump experiments with NMDA antagonists in mouse cultured hippocampal neurons. J Neurophysiol 63:1373–1384.

Busch C, Sakmann B (1990) Synaptic transmission in hippocampal neurons: numerical reconstruction of quantal IPSCs. Cold Spring Harb Symp Quant Biol 55:69–80.

Celentano JJ, Wong RKS (1994) Multiphasic desensitization of the $GABA_A$ receptor in outside-out patches. Biophys J 66:1039–1050.

Chambon JP, Feltz P, Heaulme M, Restle S, Schlichter R, Biziere K, Wermuth CG (1985) An arylaminopyridazine derivative of γ-aminobutyric acid (GABA) is a selective and competitive antagonist at the $GABA_A$ receptor. Proc Natl Acad Sci USA 82:1832–1836.

Clements JD, Westbrook GL (1991) Activation kinetics reveal the number of glutamate and glycine binding sites on the *N*-methyl-D-aspartate receptor. Neuron 7:605–613.

Clements JD, Lester RA, Tong G, Jahr CE, Westbrook GL (1992) The time course of glutamate in the synaptic cleft. Science 258:1498–1501.

Clements JD, Feltz A, Sahara Y, Westbrook GL (1998) Activation kinetics of AMPA receptor channels reveal the number of functional agonist binding sites. J Neurosci 18:119–127.

Colquhoun D, Ogden DC (1988) Activation of ion channels in the frog end-plate by high concentrations of acetylcholine. J Physiol (Lond) 395:131–159.

Colquhoun D, Sakmann B (1985) Fast events in single-channel currents activated by acetylcholine and its analogues at the frog muscle end-plate. J Physiol (Lond) 369:501–557.

Colquhoun D, Large WA, Rang HP (1977) An analysis of the action of a false transmitter at the neuromuscular junction. J Physiol (Lond) 266:361–395.

Constanti A (1977a) A quantitative study of the γ-aminobutyric acid (GABA) dose/conductance relationship at the lobster inhibitory neuromuscular junction. Neuropharmacology 16:357–366.

Constanti A (1977b) Comparison of dose/conductance curves for GABA and some structurally related compounds at the lobster inhibitory neuromuscular junction. Neuropharmacology 16:367–374.

Dennis M, Giraudat J, Kotzyba-Hibert F, Goeldner M, Hirth C, Chang JY, Lazure C, Chretien M, Changeux JP (1988) Amino acids of the *Torpedo marmorata* acetylcholine receptor alpha subunit labeled by a photoaffinity ligand for the acetylcholine binding site. Biochemistry 27:2346–2357.

Diamond JS, Jahr CE (1997) Transporters buffer synaptically released glutamate on a submillisecond time scale. J Neurosci 17:4672–4687.

Dionne VE, Steinbach JH, Stevens CF (1978) An analysis of the dose-response relationship at voltage-clamped frog neuromuscular junctions. J Physiol (Lond) 281:421–444.

Eyring H (1935) The activated complex in chemical reactions. J Chem Phys 3:107–115.

Franke C, Parnas H, Hovav G, Dudel J (1993) A molecular scheme for the reaction between acetylcholine and nicotinic channels. Biophys J 64:339–356.

Freifelder D (1982) Principles of physical chemistry with applications to the biological sciences, 2nd Ed. Boston: Jones and Bartlett.

Frerking M, Wilson M (1996) Saturation of postsynaptic receptors at central synapses? Curr Opin Neurobiol 6:395–403.

Galarreta M, Hestrin S (1997) Properties of $GABA_A$ receptors underlying inhibitory synaptic currents in neocortical pyramidal neurons. J Neurosci 17:7220–7227.

Hamann H, Desarmenien M, Desaulles E, Bader MF, Feltz P (1988) Quantitative evaluation of the properties of a pyridazinyl GABA derivative (SR 95531) as a $GABA_A$ competitive antagonist. An electrophysiological approach. Brain Res 442:287–296.

Häusser M, Roth A (1997) Dendritic and somatic glutamate receptor channels in rat cerebellar Purkinje cells. J Physiol (Lond) 501:77–95.

Hille B (1992) Ionic channels of excitable membranes, 2nd Ed. Sunderland, MA; Sinauer.

Huang J-H, Johnston GAR (1990) (+)-Hydrastine, a potent competitive antagonist at mammalian $GABA_A$ receptors. Br J Pharmacol 99:727–730.

Isaacson JS, Solis JM, Nicoll RA (1993) Local and diffuse synaptic actions of GABA in the hippocampus. Neuron 10:165–175.

Jackson MB (1989) Perfection of a synaptic receptor: kinetics and energetics of the acetylcholine receptor. Proc Natl Acad Sci USA 86:2199–2203.

Jonas P, Major G, Sakmann B (1993) Quantal components of unitary EPSCs at the mossy fibre synapse on CA3 pyramidal cells of rat hippocampus. J Physiol (Lond) 472:615–663.

Jonas P, Bischofberger J, Sandkuhler J (1998) Corelease of two fast neurotransmitters at a central synapse. Science 281:419–424.

Jones MV, Westbrook GL (1995) Desensitized states prolong $GABA_A$ channel responses to brief agonist pulses. Neuron 15:181–191.

Jones MV, Westbrook GL (1996) The impact of receptor desensitization on fast synaptic transmission. Trends Neurosci 19:96–101.

Jones MV, Westbrook GL (1997) Shaping of IPSCs by endogenous calcineurin activity. J Neurosci 17:7626–7633.

Katz B, Miledi R (1973) The binding of acetylcholine to receptors and its removal from the synaptic cleft. J Physiol (Lond) 231:549–574.

Lauffer MA (1989) Motion in biological systems. New York: Liss.

Lavoie AM, Twyman RE (1996) Direct evidence for diazepam modulation of $GABA_A$ receptor microscopic affinity. Neuropharmacology 35:1383–1392.

Lavoie AM, Tingey JJ, Harrison NL, Pritchett DB, Twyman RE (1997) Activation and deactivation rates of recombinant $GABA_A$ receptor channels are dependent on α-subunit isoform. Biophys J 73:2518–2526.

Lester RA, Jahr CE (1992) NMDA channel behavior depends on agonist affinity. J Neurosci 12:635–643.

Lester RAJ, Clements JD, Westbrook GL, Jahr CE (1990) Channel kinetics determine the time course of NMDA receptor-mediated synaptic currents. Nature 346:565–567.

Macdonald RL, Rogers CJ, Twyman RE (1989) Kinetic properties of the $GABA_A$ receptor main conductance state of mouse spinal neurones in culture. J Physiol (Lond) 410:479–499.

Magleby KL, Stevens CF (1972) A quantitative description of end-plate currents. J Physiol (Lond) 223:173–197.

Maksay G (1994) Thermodynamics of γ-aminobutyric acid type A receptor binding differentiate agonists from antagonists. Mol Pharmacol 46:386–390.

Marcus RA (1964) Generalization of the activated complex theory of reaction rates. II. Classical mechanical treatment. J Chem Phys 41:2624–2633.

Morris GM, Goodsell DS, Huey R, Olson AJ (1996) Distributed automated docking of flexible ligands to proteins: parallel applications of AutoDock 2.4. J Comp Aid Mol Design 10:293–304.

Nelder A, Mead R (1965) A simplex method for function minimization. Computer J 7:308–313.

Nusser Z, Cull-Candy S, Farrant M (1997) Differences in synaptic $GABA_A$ receptor number underlie variation in GABA mini amplitude. Neuron 19:697–709.

Pallotta BS (1991) Single ion channel's view of classical receptor theory. FASEB J 5:2035–2043.

Pan ZZ, Tong G, Jahr CE (1993) A false transmitter at excitatory synapses. Neuron 11:85–91.

Papke RL, Millhauser G, Lieberman Z, Oswald RE (1988) Relationships of agonist properties to the single channel kinetics of nicotinic acetylcholine receptors. Biophys J 53:1–10.

Perrais D, Ropert N (1997) Effects of zolpidem on mIPSCs and occupancy of $GABA_A$ receptors in central synapses. Soc Neurosci Abstr 23:377.

Puia G, Costa E, Vicini S (1994) Functional diversity of GABA-activated Cl^- currents in Purkinje versus granule neurons in rat cerebellar slices. Neuron 12:117–126.

Raman IM, Trussell LO (1995) The mechanism of α-amino-3-hydroxy-5-methyl-4-isoxazolepropionate receptor desensitization after removal of glutamate. Biophys J 68:137–146.

Schmieden V, Kuhse J, Betz H (1992) Agonist pharmacology of neonatal and adult glycine receptor α subunits: identification of amino acid residues involved in taurine activation. EMBO J 11:2025–2032.

Schmieden V, Kuhse J, Betz H (1993) Mutation of glycine receptor subunit creates β-alanine receptor responsive to GABA. Science 262:256–258.

Segel I (1976) Biochemical calculations, 2nd Ed. New York: Wiley.

Sine SM, Steinbach JH (1986) Activation of acetylcholine receptors on clonal mammalian BC3H-1 cells by low concentrations of agonist. J Physiol (Lond) 373:129–162.

Sine SM, Ohno K, Bouzat C, Auerbach A, Milone M, Pruitt JN, Engel AG (1995) Mutation of the acetylcholine receptor α subunit causes slow-channel myasthenic syndrome by enhancing agonist binding affinity. Neuron 15:229–239.

Smith GB, Olsen RW (1995) Functional domains of $GABA_A$ receptors. Trends Pharmacol 16:162–168.

Stern-Bach Y, Bettler B, Hartley M, Sheppard PO, O'Hara PJ, Heinemann SF (1994) Agonist selectivity of glutamate receptors is specified by two domains structurally related to bacterial amino acid-binding proteins. Neuron 13:1345–1357.

Tia S, Wang JF, Kotchabhakdi N, Vicini S (1996) Developmental changes of inhibitory synaptic currents in cerebellar granule neurons: role of $GABA_A$ receptor α6 subunit. J Neurosci 16:3630–3640.

Twyman RE, Rogers CJ, Macdonald RL (1990) Intraburst kinetic properties of the $GABA_A$ receptor main conductance state of mouse spinal chord neurons in culture. J Physiol (Lond) 423:193–220.

Ueno S, Bracamontes J, Zorumski C, Weiss DS, Steinbach JH (1997) Bicuculline and gabazine are allosteric inhibitors of channel opening of the $GABA_A$ receptor. J Neurosci 17:625–634.

Vandenberg RJ, Handford CA, Schofield PR (1992) Distinct agonist- and antagonist-binding sites on the glycine receptor. Neuron 9:491–496.

Verdoorn TA (1994) Formation of heteromeric $GABA_A$ receptors containing two different alpha subunits. Mol Pharmacol 45:475–480.

Wentworth WE, Ladner SJ (1972) Fundamentals of physical chemistry. Belmont, CA: Wadsworth.

Zhang Y, Chen J, Auerbach A (1995) Activation of recombinant mouse acetylcholine receptors by acetylcholine, carbamylcholine and tetramethylammonium. J Physiol (Lond) 486:189–206.